Nonlinear time-dependent simulation of helix traveling wave tubes*

Peng Wei-Feng(彭维峰), Yang Zhong-Hai(杨中海), Hu Yu-Lu(胡玉禄), Li Jian-Qing(李建清), Lu Qi-Ru(陆麒如), and Li Bin(李 斌)†

Vacuum Electronics National Laboratory, University of Electronic Science and Technology of China, Chengdu 610054, *China*

(Received 13 October 2010; revised manuscript received 17 January 2011)

A one-dimensional nonlinear time-dependent theory for helix traveling wave tubes is studied. A generalized electromagnetic field is applied to the expression of the radio frequency field. To simulate the variations of the high frequency structure, such as the pitch taper and the effect of harmonics, the spatial average over a wavelength is substituted by a time average over a wave period in the equation of the radio frequency field. Under this assumption, the space charge field of the electron beam can be treated by a space charge wave model along with the space charge coefficient. The effects of the radio frequency and the space charge fields on the electrons are presented by the equations of the electron energy and the electron phase. The time-dependent simulation is compared with the frequency-domain simulation for a helix TWT, which validates the availability of this theory.

Keywords: helix traveling wave tubes, time-dependent, harmonics, helix pitch taper

PACS: 84.40.Fe, 13.40.Ks **DOI:** 10.1088/1674-1056/20/7/078401

1. Introduction

Helix traveling wave tubes (TWTs) can provide radio frequency (RF) augmentation with wide bandwidth and high efficiency. Helix TWTs are becoming more in demand for space tubes and in high date rate communications. The research into helix TWTs has been going on since the pioneering work of Pierce and his coworkers.[1] There is growing literature on the simulation of helix TWTs with beam–wave interaction (BWI).[2] These theories can be categorized as frequency-domain[3−5] and time-dependent[6−8] analyses. The time-dependent models are usually more computationally intensive than the frequency-domain ones. The time-dependent models have some advantages. The most significant one is that the time-dependent models can treat temporally varying inputs and outputs with complex waveforms or pulse shapes.

In this paper, a one-dimensional (1D) time-dependent theory for helix TWTs is presented. The slow wave structure (SWS) of the helix is modeled by a sheath helix, and the electromagnetic fields are expressed in the representation of the assumed fields of the vacuum structure and in the form of the product of slowly varying complex amplitudes, eigenfunctions and an exponential phase factor. The spatial average over a wavelength is substituted by a time average over a wave period, which has been used in the equation of the radio frequency field in the frequency domain. The most important advantage of the substitution for the spatial average is that a time average makes it easier to treat harmonics and the helix taper. To calculate the space charge (SC) fields of electrons, the interaction space is divided into disjoint regions with generalized beam boundary conditions. We separate the field solution of the Maxwell's equations with sources into the part with the shape of the vacuum fields (i.e. RF fields) and the residual part. The residual part will be the SC fields, which are matched to the beam boundary conditions. By combining the RF and the SC fields with equations of motion, the self-consistent BWI simulating equations are obtained

The organization of the rest of the paper is as follows. In Section 2, the general formulation of RF fields, SC fields and electron motion is described. A numerical analysis of a helix TWT is given in Section 3. A comparison between the results obtained from the time-dependent and the frequency-domain[9] simulations is made in this section too. The conclusion is given in Section 4.

*Project supported by the National Natural Science Foundation of China (Grant Nos. 60601004, 60801029, 10876005, and 60931001).

†Corresponding author. E-mail: libin@uestc.edu.cn

© 2011 Chinese Physical Society and IOP Publishing Ltd

2. Physical model

A physical model treating the propagation of multiple RF signals through a helix SWS in the presence of an electron beam is presented in this section. Both RF and SC fields are described by their corresponding equations. The equation of motion is also included.

2.1. RF fields

The so-called RF fields are the fields of the structure described in the representation of the assumed fields of the cold structure (i.e., in the absence of the beam). The RF fields are given in terms of electromagnetic fields $\boldsymbol{E}_{\rm rf}$ and $\boldsymbol{B}_{\rm rf}$, which are then expressed in the form of the product of the temporally and spatially slowly varying complex amplitude δA_n, the eigenfunctions $\boldsymbol{e}_n(\boldsymbol{x})$ and $\boldsymbol{b}_n(\boldsymbol{x})$, and a phase factor[4,5] as follows

$$\begin{aligned}\boldsymbol{E}_{\rm rf} &= \sum_n {\rm i}\frac{\omega_n}{c}\delta A_n(z,t)\,\boldsymbol{e}_n(\boldsymbol{x}) \\ &\quad\times\exp\left[{\rm i}\left(\int_0^z k_{zn}(z')\,{\rm d}z'-\omega_n t\right)\right]+{\rm c.c.}, \quad (1)\\ \boldsymbol{B}_{\rm rf} &= \sum_n {\rm i}\frac{\omega_n}{c}\delta A_n(z,t)\,\boldsymbol{b}_n(\boldsymbol{x}) \\ &\quad\times\exp\left[{\rm i}\left(\int_0^z k_{zn}(z')\,{\rm d}z'-\omega_n t\right)\right]+{\rm c.c.} \quad (2)\end{aligned}$$

The summations in Eqs. (1) and (2) run over frequencies labeled by the subscript n. The eigenfunctions are solutions of the Maxwell's equations for the cold structure corresponding to the angular frequency ω_n. The parameter c is the speed of light in vacuum, and c.c. takes the conjugate of the former terms.

To account for the influence of the slow structure variation on the amplitudes of the RF fields, the temporally and axially spatially varying normalized field amplitude is introduced as

$$a_n(z,t)=\frac{\omega_n}{c}\frac{q_0\delta A_n(z,t)}{m_0c^2}A_{{\rm eff},n}^{1/2}(z), \quad (3)$$

where q_0 and m_0 are the charge and the mass of a rest electron, respectively, and $A_{{\rm eff},n}$ denotes the effective power of the cross-section area and is give by

$$\begin{aligned}A_{{\rm eff},n}(z) &= \frac{1}{2}\iint_S {\rm d}^2x_\perp\boldsymbol{z}\cdot[\boldsymbol{e}_n(\boldsymbol{x})\times\boldsymbol{b}_n^*(\boldsymbol{x}) \\ &\quad+\boldsymbol{e}_n^*(\boldsymbol{x})\times\boldsymbol{b}_n(\boldsymbol{x})]. \quad (4)\end{aligned}$$

The power p_n of the n-th signal can be expressed as

$$p_n=\frac{c}{2\pi}\left(\frac{m_0c^2}{q_0}\right)^2|a_n(z,t)|^2=P_{{\rm flux},2}\,|a_n(z,t)|^2, \quad (5)$$

where

$$P_{{\rm flux},2}=\frac{c}{2\pi}\left(\frac{m_0c^2}{q_0}\right)^2=1.3862\times10^9\ {\rm W}$$

is a constant in the MKS system of units. The total power $p_{\rm all}$ of all signals existing in the structure is

$$p_{\rm all}=P_{{\rm flux},2}\sum_n|a_n(z,t)|^2. \quad (6)$$

The time-averaged energy density W_n of a signal with angular frequency ω_n in unit axial length and over the entire cross section of the structure is

$$\begin{aligned}W_n &= \frac{1}{4\pi}\left|\frac{\omega_n\delta A_n(z,t)}{c}\right|^2\iiint_V[\boldsymbol{e}_n(\boldsymbol{x})\cdot\boldsymbol{e}_n^*(\boldsymbol{x}) \\ &\quad+\boldsymbol{b}_n(\boldsymbol{x})\cdot\boldsymbol{b}_n^*(\boldsymbol{x})]{\rm d}V \\ &= P_{{\rm flux},2}\,|a_n(z,t)|^2\frac{A_{{\rm eff},n}}{U_{{\rm eff},n}}, \quad (7)\end{aligned}$$

where $U_{{\rm eff},n}$ denotes the effective energy of the cross-section area and is given as

$$\begin{aligned}U_{{\rm eff},n}(z) &= \frac{1}{2c}\iint_S {\rm d}^2x_\perp[\boldsymbol{e}_n(\boldsymbol{x})\cdot\boldsymbol{e}_n^*(\boldsymbol{x}) \\ &\quad+\boldsymbol{b}_n(\boldsymbol{x})\cdot\boldsymbol{b}_n^*(\boldsymbol{x})]. \quad (8)\end{aligned}$$

The group speed of the n-th signal is

$$v_{{\rm gr},n}=p_n/W_n=A_{{\rm eff},n}/U_{{\rm eff},n}. \quad (9)$$

The equations for the complex amplitudes are derived in the following. Expressions (1) and (2) are substituted into the Maxwell's equations with a current density $\boldsymbol{j}$. Ampere's law and Faraday's law are dotted with $\boldsymbol{e}_n(\boldsymbol{x})$ and $\boldsymbol{b}_n(\boldsymbol{x})$, respectively. Combining the two products in the same way as that of Poynting's theorem yields

$$\begin{aligned}&\sum_n\left[\nabla\frac{a_n(z,t)}{A_{{\rm eff},n}^{1/2}}\times\boldsymbol{e}_n(\boldsymbol{x},t)\right. \\ &\left.+\frac{\boldsymbol{b}_n(\boldsymbol{x},t)}{A_{{\rm eff},n}^{1/2}}\frac{1}{c}\frac{\partial a_n(z,t)}{\partial t}\right]+{\rm c.c.}=0, \quad (10)\\ &\sum_n\left[\nabla\frac{a_n(z,t)}{A_{{\rm eff},n}^{1/2}}\times\boldsymbol{b}_n(\boldsymbol{x},t)\right. \\ &\left.-\frac{\boldsymbol{e}_n(\boldsymbol{x},t)}{A_{{\rm eff},n}^{1/2}}\frac{1}{c}\frac{\partial a_n(z,t)}{\partial t}\right]+{\rm c.c.}=-{\rm i}\frac{4\pi}{I_{\rm A}}\boldsymbol{j}, \quad (11)\end{aligned}$$

where $I_{\rm A}=m_0c^3/q_0=1.7033\times10^4$ A is a constant. By averaging the Eqs. (10) and (11) over a temporal period T, the equation for the amplitude of the n-th signal can be given as

$$\left[v_{{\rm gr},n}\frac{\partial}{\partial z}+v_{{\rm gr},n}\alpha_n(z)+\frac{\partial}{\partial t}\right]a_n(z,t)$$

$$= \mathrm{i}\,\frac{2\pi}{I_\mathrm{A}}\frac{v_{\mathrm{gr},n}}{A_{\mathrm{eff},n}^{1/2}}\left\langle \iint\limits_S \mathrm{d}^2x_\perp \boldsymbol{j}\cdot\boldsymbol{e}_n^*(\boldsymbol{x},t)\right\rangle_T, \quad (12)$$

where $\alpha_n(z) = -0.5A_{\mathrm{eff},n}^{-1}\partial_z A_{\mathrm{eff},n}(z)$ is the circuit loss rate, and the expression for the eigenfunction is given as

$$\boldsymbol{e}_n(\boldsymbol{x},t) = \boldsymbol{e}_n(\boldsymbol{x})\exp\left[\mathrm{i}\left(\int_0^z k_{zn}(z')\,\mathrm{d}z' - \omega_n t\right)\right].$$

The angular bracket denotes the time averaging over T. Note that the temporal period is $T = 2\pi/\omega_n$ for a single signal, while $T = 2\pi/\Delta\omega$ for multiple signals, where $\Delta\omega$ is the greatest common divisor for all angular frequencies in the SWS.

In the 1D model, the beam is treated as angular rings each with outer radius r_bo and inner radius r_bi moving along the axial direction only. In this model, the current density can be expressed[6–8] as

$$j_z = \sum_j q_j v_{j,z}(t)\frac{S[z-z_j(t)]}{\pi(r_\mathrm{bo}^2 - r_\mathrm{bi}^2)}, \quad (13)$$

where summation runs over all particles in the structure at time t and at the grid position z, the parameters $v_{j,z}$ and q_j are the axial velocity and the charge of the j-th particle, respectively. The interpolating function is

$$S[z-z_j(t)] = \begin{cases} (z - z_j + \Delta z)/\Delta z^2, & z_j - \Delta z \le z \le z_j, \\ (\Delta z + z_j - z)/\Delta z^2, & z_j < z \le z_j + \Delta z. \end{cases} \quad (14)$$

Substituting Eq. (14) into Eq. (12), the RF equation can be rewritten in the 1D form as

$$\left[v_{\mathrm{gr},n}\frac{\partial}{\partial z} + v_{\mathrm{gr},n}\alpha_n(z) + \frac{\partial}{\partial t}\right]a_n(z,t)$$
$$= \mathrm{i}\,\frac{2\pi v_{\mathrm{gr},n}}{I_\mathrm{A}}\sum_j q_j v_{j,z}(t)\,S[z-z_j(t)]$$
$$\times\left\langle \frac{1}{A_{\mathrm{eff},n}^{1/2}S_\mathrm{beam}}\iint\limits_S \mathrm{d}^2x_\perp \boldsymbol{e}_n^*(\boldsymbol{x},t)\right\rangle_T, \quad (15)$$

where the parameter $S_\mathrm{beam} = \pi\left(r_\mathrm{bo}^2 - r_\mathrm{bi}^2\right)$ is the averaged cross-section area of the beam. The right integral of Eq. (15) can be called as the RF field coupling source, which is directly related to the coupling impedance $K_{\mathrm{c},n}(r)$ in the form of

$$K_{\mathrm{c},n}(r) = |\boldsymbol{z}\cdot\boldsymbol{e}_n(r)|^2\Big/\left(\frac{c}{4\pi}k_{zn}^2 A_{\mathrm{eff},n}\right). \quad (16)$$

Averaging Eq. (16) over S_beam and substituting the integral result into Eq. (15), the RF equation can be packed up as

$$\left[v_{\mathrm{gr},n}\frac{\partial}{\partial z} + v_{\mathrm{gr},n}\alpha_n(z) + \frac{\partial}{\partial t}\right]a_n(z,t)$$
$$= \mathrm{i}\,C_n\left\langle \frac{T}{N_\lambda}\sum_j v_{j,z}(t)\,S[z-z_j(t)]\right.$$
$$\left.\times\exp\left[-\mathrm{i}\left(\int_0^z k_{zn}(z')\,\mathrm{d}z' - \omega_n t\right)\right]\right\rangle_T, \quad (17)$$

where

$$C_n = \frac{2\pi I_\mathrm{b} k_{zn} v_{\mathrm{gr},n}}{I_\mathrm{A}}\frac{2\left[\gamma_n r \mathrm{I}_1(\gamma_n r)\right]_{R_\mathrm{bi}}^{R_\mathrm{bo}}}{\gamma_n^2\left(r_\mathrm{bo}^2 - r_\mathrm{bi}^2\right)}\sqrt{\frac{K_{\mathrm{c},n}(z,0)}{377\Omega}}$$

is a coefficient, and N_λ is the number of particles entering into the SWS in the time scale of T. The propagating factor γ_n is calculated as $\gamma_n^2 = k_{zn}^2 - \omega_n^2/c^2$. The $K_{\mathrm{c},n}(z,0)$ is the on-axis coupling impedance at position z for the n-th signal. The $\mathrm{I}_1(\gamma_n r)$ is the first order modified Bessel function.

The normalized field amplitude $a_n(z,t)$ can be calculated by solving the real and the image parts of Eq. (17), so the varying RF fields at different position z and time t can be obtained. Here, the parameters $K_{\mathrm{c},n}(z,0)$ and $v_{\mathrm{gr},n}$ can be calculated first by using the computational electromagnetic code, such as the HFSS.[10]

2.2. SC Fields

The temporally and spatially varying RF electric fields expressed in expression (1) satisfy the Maxwell's equations in the absence of the beam but cannot satisfy the Maxwell's equations with the source charge and the current densities by themselves. In the actual situation with the beam loaded, an additional field should be presented in the structure. The additional part, which is usually called the SC field, can be calculated in the following way. First, transform the source charge and the current densities into wave forms by the Fourier transformation. Second, substitute the wave sources and the fields of the cold structure into the Maxwell's equations. Finally, by extracting the RF fields from the total fields, the fluctuating part of the SC field (i.e. AC SC field) is obtained. At the

same time, the effect of the direct part of the SC field (i.e. DC SC field) is included in the initial speed of the beam ring.

By using the Fourier factor $\psi^{(\mathrm{e})} = k_z^{(\mathrm{e})} z - \omega t$, the sources and the total fields $\boldsymbol{E}$ and $\boldsymbol{B}$ existing in the structure can be transformed into

$$\begin{aligned} j_z &= j_{z0} + \frac{I}{\pi\,(r_{\mathrm{bo}}^2 - r_{\mathrm{bi}}^2)} \\ &\quad \times \left[\sum_{l=1}^{\infty} \exp\left(\mathrm{i}\, l\psi^{(\mathrm{e})}\right) \left\langle \exp\left(-\mathrm{i}\, l\psi^{(\mathrm{e})}\right)\right\rangle_T \right. \\ &\quad \left. + \mathrm{c.c.}\right], \end{aligned} \tag{18}$$

$$\begin{aligned} \rho &= \rho_0 + \frac{I}{\pi\,(r_{\mathrm{bo}}^2 - r_{\mathrm{bi}}^2)} \frac{k_z^{(\mathrm{e})}}{\omega} \\ &\quad \times \left[\sum_{l=1}^{\infty} \exp\left(\mathrm{i}\, l\psi^{(\mathrm{e})}\right) \left\langle \exp\left(-\mathrm{i}\, l\psi^{(\mathrm{e})}\right)\right\rangle_T \right. \\ &\quad \left. + \mathrm{c.c.}\right], \end{aligned} \tag{19}$$

$$\boldsymbol{E} = \boldsymbol{E}_0 + \sum_{l=1}^{\infty} \left[\boldsymbol{E}_l \exp\left(\mathrm{i}\, l\psi^{(\mathrm{e})}\right) + \mathrm{c.c.}\right], \tag{20}$$

$$\boldsymbol{B} = \boldsymbol{B}_0 + \sum_{l=1}^{\infty} \left[\boldsymbol{B}_l \exp(\mathrm{i}\, l\psi^{(\mathrm{e})}) + \mathrm{c.c.}\right], \tag{21}$$

where $k_z^{(e)} = \omega / v_{z0}$ is the wave number of the electron beam. The subscripts 0 and l denote the direct current part and the l-th part of the physical parameters, respectively. Substituting Eqs. (18) and (21) into the Maxwell's equations, the Helmholtz equations are given as

$$\boldsymbol{\nabla}^2 \boldsymbol{E} - \frac{1}{c^2} \frac{\partial^2 \boldsymbol{E}}{\partial^2 t} = \frac{-\mathrm{i}\, 4\pi}{\omega} \left(\frac{\partial^2}{\partial z^2} + \frac{\omega^2}{c^2} \right) j_z \hat{\boldsymbol{z}}, \tag{22}$$

$$\boldsymbol{\nabla}^2 \boldsymbol{B} - \frac{1}{c^2} . \frac{\partial^2 \boldsymbol{B}}{\partial^2 t} = 0. \tag{23}$$

The boundary conditions for Eqs. (22) and (23) are that the fields are matched in the beam radius and the helix is made of a perfect conductor. So the total axial electric field in the area of the beam is

$$\begin{aligned} \langle E_z \rangle_{\mathrm{beam}} &= \sum_{l=1}^{\infty} \left[E_{\mathrm{rf}z,l} - \frac{\mathrm{i}\, 4I}{\omega_l\,(r_{\mathrm{bo}}^2 - r_{\mathrm{bi}}^2)} R_l \right. \\ &\quad \left. \times \langle \exp\left(-\mathrm{i}\, l\psi\right)\rangle + \mathrm{c.c.}\right], \end{aligned} \tag{24}$$

where the space charge reduction coefficient R_l is given in terms of the modified Bessel functions as

$$\begin{aligned} R_l &= 1 - \frac{2}{(r_{\mathrm{bo}}^2 - r_{\mathrm{bi}}^2)} \{ [r_{\mathrm{bo}} \mathrm{K}_1(\gamma_l r_{\mathrm{bo}}) \\ &\quad + \mathrm{K}_0(\gamma_l r_h) r \mathrm{I}_1(\gamma_l r)|_{r_{\mathrm{bi}}}^{r_{\mathrm{bo}}} / \mathrm{I}_0(\gamma_l r_h)] \cdot (r \mathrm{I}_1(\gamma_l r)|_{r_{\mathrm{bi}}}^{r_{\mathrm{bo}}}) \\ &\quad - r_{\mathrm{bi}} \mathrm{I}_1(\gamma_l r_{\mathrm{bi}}) (r \mathrm{K}_1(\gamma_l r)|_{r_{\mathrm{bi}}}^{r_{\mathrm{bo}}}) \}, \end{aligned} \tag{25}$$

The $\psi^{(\mathrm{e})}$ is substituted by $\psi = k_z z - \omega t$ when the l-th axial RF field $E_{\mathrm{rf}z,l}$ is extracted from the total field E_z under the assumption of $k_z^{(\mathrm{e})} \to k_z$. The angular bracket combining with the subscript beam denotes taking average over the cross-section area of the beam. So the AC SC field can be given as

$$\begin{aligned} \langle E_{\mathrm{sc},z} \rangle_{\mathrm{beam}} &= -\sum_n \sum_l \frac{\mathrm{i}\, 4I}{\omega_{n,l}(r_{\mathrm{bo}}^2 - r_{\mathrm{bi}}^2)} R_{n,l} \\ &\quad \times \langle \exp(-\mathrm{i}\, l\psi_n)\rangle \exp(\mathrm{i}\, l\psi_n) + \mathrm{c.c.} \end{aligned} \tag{26}$$

where the summation of n runs over all signals, and l is over all harmonics of the n-th signal. The value of the phase average is given as

$$\langle \exp(-\mathrm{i}\, l\psi) \rangle = \frac{1}{N_\lambda} \sum_{j=1}^{N_\lambda} \exp[-\mathrm{i}\, l(k_z z - \omega t)], \tag{27}$$

which can be seen as a stimulating source at position z and time t, where N_λ is the number of the electron passing through z in the time range $[t, t+T]$. The interpolating function described in expression (14) is added into expression (27) for the axial grids, as the electrons are filled in the structure during the course of BWI.

2.3. Equations of motion

In the 1D model, the electron beam is treated as rings or discs of charge, each with inner and outer radii r_{bo} and r_{bi}, respectively. The axial speed v_z of a ring or a disc is related to its relativistic factor $\gamma = 1/\sqrt{1 - v_z^2/c^2}$ by

$$\frac{\mathrm{d}\gamma}{\mathrm{d}t} = \frac{v_z \eta}{c^2} (E_{\mathrm{rf},z} + E_{\mathrm{sc},z}), \tag{28}$$

where η is the charge-to-mass ratio of a rest electron. The electron position z is related to v_z by

$$\frac{\mathrm{d}z}{\mathrm{d}t} = v_z. \tag{29}$$

In the time-domain model, the independent variables of the equation of motion are time t and position z, so the phase factor $\psi = k_z z - \omega t$ existing in field Eqs. (17) and (26) can be directly calculated. In the 1D beam, the DC SC field E_{dc} can be given in the form of a function of radial position r as

$$E_{\mathrm{dc}} = -\frac{I}{2\pi\varepsilon_0 v_{z0}} \begin{cases} r/r_{\mathrm{b}}^2, & 0 \le r < r_{\mathrm{bo}}, \\ 1/r, & r \ge r_{\mathrm{b}}, \end{cases} \tag{30}$$

where ε_0 is the dielectric constant in the vacuum, and v_{z0} is the initial axial speed of an electron. Integrating expression (30) in the radial range of $[0, r_{\mathrm{h}}]$, the

difference between the beam voltage $V_{\rm b}$ and the helix voltage $V_{\rm h}$ is given by the depression voltage ΔV as

$$\Delta V = |V_{\rm h} - V_{\rm b}| = 1.52 \times 10^4 \frac{I}{V_{\rm h}^{1/2}}[1 + 2\ln(r_{\rm h}/r_{\rm b})]. \quad (31)$$

So the initial relativistic factor γ_0 for each electron is given by

$$\gamma_0 = \frac{\eta}{c^2}(V_{\rm h} - \Delta V). \quad (32)$$

The final self-consistent equations for the 1D time-domain model can be given by the combination of Eqs. (17), (26), (28) and (29). In solving the simultaneous equations, a set of grids with the electrons uniformly distributed in them are set up so as to treat the moving course of the electrons from the gun to the collector.

3. Numerical results

The sequence for simulation using this 1D time-dependent theory is as follows. First, set the initial conditions. The electrons are uniformly distributed in the structure, and both RF and SC fields are zero at each grid. Second, the signals with temporally varied amplitudes are injected. The stimulating sources for the RF field equations and for the SC field equations are calculated by accumulating electron charges to the grid and averaging over the scale of a time period. Third, the SC fields are calculated directly while the RF fields are calculated by using the MacCormack method. Fourth, the trajectories for the electrons are calculated by solving the equations of motion using the fourth-order Runge-Kutta method. The procedure is repeated over the time scale.

The SWS chosen to be simulated is a helix TWT built by the Northrop–Grumman Corporation. The average radius and the pitch of the helix are 1.245 mm and 0.8014 mm, respectively. The wall radius is 2.794 mm. No vane is loaded in the structure. There are three rods with rectangular cross sections running along the helix. The dielectric constants of the rods are all 6.5 and their crosssection dimensions are all 0.508 mm×1.473 mm. The helix voltage, the electron beam current and the fill-ratio (i.e. the ratio of the beam radius to the helix radius) are 2.84 kV, 170 mA, and 0.5, respectively.

A plot for the evolution of the input power with time is shown in Fig. 1. In this paper, two kinds of input powers are chosen to be simulated. One is an input power of the continuous type. In this simulation, a signal with a frequency of 5 GHz and a stabilized power of 30 mW is injected at the initial axial position of $z = 0$. The rising time for the input power is 1 ns (i.e., the input power increases up from zero to its stabilized value in 1 ns). The other is of the impulse type. In this simulation, an impulse signal with a frequency of 5 GHz and a peak power of 30 mW is injected with the delayed and the standing time of 1 ns and 2 ns, respectively. Both kinds of input powers are shown in Fig. 1 as the solid and the dashed lines, respectively.

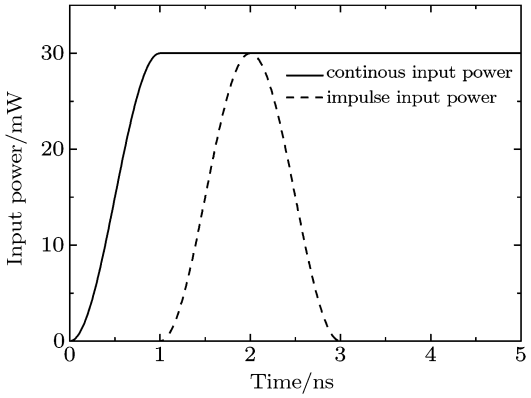


Fig. 1. Evolutions of input power with time.

The plots for the stabilized time-dependent output power varying with the axial position are shown in Figs. 2 and 3. Also included in Figs. 2 and 3 are the plots for the frequency-domain[9,11] output power varying with the axial position. It is noted that the input power for simulating the stabilized output power

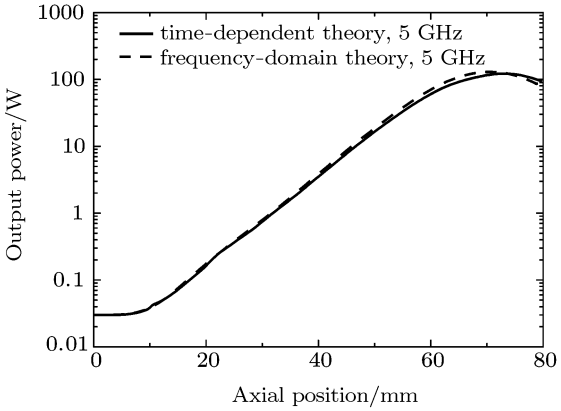


Fig. 2. Evolutions of the base frequency (i.e. 5 GHz) output power with the axial position. The solid curve corresponds to the stabilized output power of the time-dependent theory with the input power of the continuous type, the dashed curve corresponds to the output power of the frequency-domain theory.

is of the continuous type and is described in Fig. 1 by the solid line. The comparison of the base frequency output power of the time-dependent theory and the frequency-domain theory is given in Fig. 2. The comparison of the base frequency and the first harmonic output power is given in Fig. 3. The curves are so similar that there is no obvious difference between the two theories for the stabilized situation. As the frequency-domain theory of BWI is popularly used in practical calculation and simulation, this homology can prove the validity of the time-dependent theory implicitly.

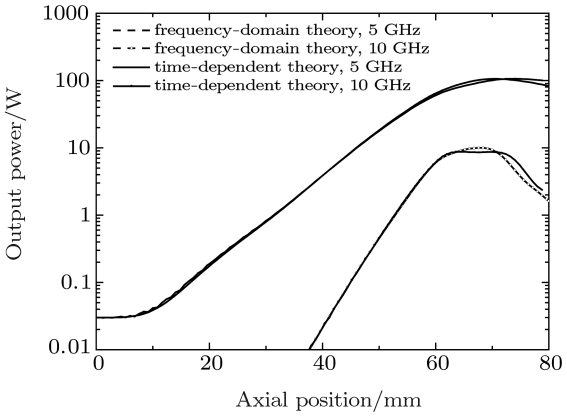


Fig. 3. Evolutions of the base frequency (i.e. 5 GHz) and its first harmonic (i.e. 10 GHz) output power with the axial position. The solid curve corresponds to the stabilized output power of the time-dependent theory with the input power of the continuous type, the dashed curve corresponds to the output power of the frequency-domain theory.

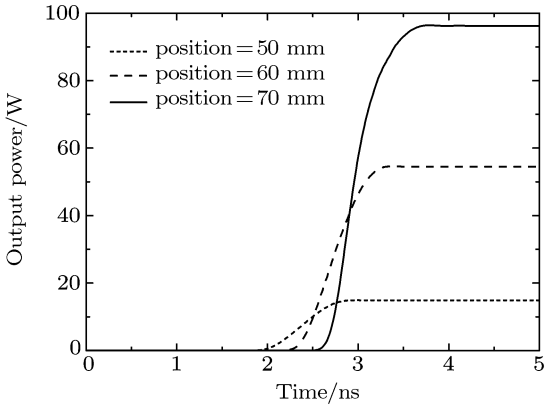


Fig. 4. Evolutions of the output power with time at the axial positions of 50 mm, 60 mm and 70 mm, respectively. The input power type for this figure is the continuous one shown in Fig. 1.

The evolutions of the output power with time at different axial positions are shown in Figs. 4 and 5. The shapes of all curves of the output power are the same as those of the input power curves in Fig. 1. The stabilized values shown in Fig. 4 are 96.3 W, 54.5 W, and 14.9 W, which are very close to the peak values of 99.2 W, 56.1 W, and 15.7 W shown in Fig. 5, respectively.

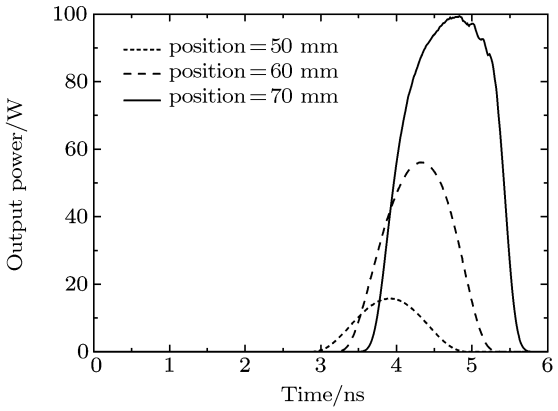


Fig. 5. Evolutions of the output power with time at the axial positions of 50 mm, 60 mm, and 70 mm, respectively. The input power type for this figure is the impulse one shown in Fig. 1.

The technology of pitch taper is usually used in helix TWTs as a way to enhance the output power. In this paper, a structure with a helix pitch taper is given in Fig. 6. The main helix pitch is 0.8014 mm for $0 \leq z \leq 70$ mm. The pitch decreases linearly to 0.68 mm at $z = 100$ mm and further decreases linearly to 0.58 mm at $z = 120$ mm which is the output position. The output power of the signal with the frequency of 5 GHz is about 210 W, which is much larger than the stabilized output power of 130 W shown in Fig. 3. Though the length of the structure is longer, the output power is notably enhanced.

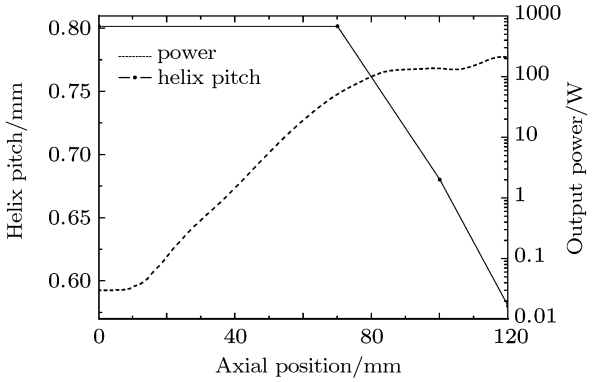


Fig. 6. Evolutions of the stabilized output power with the axial position and the shape of helix pitch taper.

4. Conclusion

A one-dimensional time-dependent nonlinear theory for helix TWTs with BWI is developed in this paper. The RF fields of the base frequency and its

harmonics are described by the generalized electromagnetic fields. The SC fields are calculated as the residual part with the RF fields extracted from the total fields, which are obtained from the Maxwell's equations with current and charge sources. The numerical results show that the time-dependent theory is able to simulate the characteristics of the BWI, such as the output power of the base frequency and of its harmonics, the effect of pitch taper. In the present work, the model for the SC fields is just a simple one. The model for the SC fields can be improved in time-dependent theories , which will be a future work. More exact models for calculating the SC fields, such as the Poisson's equations model and the particle in cell method, should be developed in the future.

References

[1] Pierce J R 1950 *Traveling Wave Tubes* (Princeton: van Nostrand) pp. 109–115

[2] Rowe J E 1956 *IRE Tran. Electron Devices* **3** 39

[3] Morey I J and Birdsall C K 1990 *IEEE Plasmas Sci.* **18** 482

[4] Chernin D P, Antonsen Jr T M, Levush B and Whaley D R 2001 *IEEE Tran. Electron Devices* **48** 3

[5] Chernin D P and Antonsen Jr T M 2003 *IEEE Tran. Electron Devices* **50** 2540

[6] Freund H P, Zaidman E G and Antonsen Jr T M 1996 *Phys. Plasmas* **3** 3145

[7] Freund H P and Zaidman E G 1997 *Phys. Plasmas* **4** 2292

[8] Freund H P 1999 *Phys. Plasmas* **6** 3633

[9] Li B, Yang Z H and Li J Q 2009 *IEEE Trans. Electron Devices* **56** 919

[10] Lee J F, Sun D K and Cendes Z J 1991 *IEEE Trans. Magn.* **27** 4032

[11] Hu Y L, Yang Z H, Li B and Li J Q 2010 *Acta Phys. Sin.* **59** 54 (in Chinese)